

## 16. NEW ACCELEROMETERS UNDER DEVELOPMENT

Dr. Jerry Wald and Dr. M. Tehrani  
Honeywell Systems and Research Center

## ABSTRACT

The commercial viability of the Space Station requires that it provide a micro-g, or submicro-g environment to users. This represents significant improvement over existing systems.

Attainment of the lowest micro-g levels requires isolation systems. Passive and active systems have been evaluated. Best performance is achieved using active approaches where accelerometer sensors close feedback loops. Available accelerometers are reviewed elsewhere in this workshop. Two emerging accelerometer technologies are presented that have promise for meeting performance goals while achieving reductions of package size, weight, and power. The technologies addressed are Honeywell's design concept for an optical cavity locking accelerometer and the recent development of an integrated silicon accelerometer for government applications.

## I. INTRODUCTION

NASA has asked its Space Station Work Package 2 contractor to evaluate the Space Station accommodation of acceleration environments needed for (1) scientific research, including materials processing in space (MPS) and life sciences; (2) engineering research and development of MPS, commercial preproduction scale-up of MPS and; (3) commercial production of material products. Mission data developed at the second Hampton Workshop showed science and commercial requirements for  $10^{-5}g$ . Subsequent analyses showed, first, a need for  $10^{-6}g$  or better, and second, that previous spacecraft (including Skylab, Shuttle, Spacelab, Soyuz) provided better performance than initial Space Station configurations because experiments are or were conducted close to the vehicles'

centers of gravity. These findings resulted in new analyses to assess the impact of payloads requiring  $\leq 10^{-6}g$  for extended periods on Space Station design.

## II. ANALYSES AND RESULTS

NASA required that three options be addressed. The options are summarized in Table 1.

MPS requirements (including microgravity and cycle time requirements), MPS tolerance to accelerations and effects of disturbance sources have been investigated to determine if the NASA options can be met. Representative microgravity requirements related to processes are shown in Figure 1.

Acceleration responses for disturbance sources were analyzed and characterized, including crew motion, coarse pointing system and docking. Crew disturbance transfer functions were investigated. In addition, events, such as MRMS operation, reboost, and steady-state orbital effects, were considered. Typical disturbance envelopes appear in Figure 2. Based on the analyses performed, achievement of  $10^{-5}g$  is limited by reboost and berthing operations and by crew motion;  $10^{-6}g$  by venting, plume impingement, module placement and CG excursions;  $10^{-7}$  by aerodynamics, air flow and sensor/servo errors. It has been concluded, however, that the micro-g environment looks achievable for extended time periods between major Space Station operation (e.g., docking, reboost, MRMS) if a mission equipment isolation system is used. One-tenth of a micro-g may be possible, but this will require tight center-of-gravity control, restrict scheduling to quiet sun periods or require continuous low thrust, restricts crew exercise for short periods, and requires a low-frequency isolation system.

The design of the isolator is influenced by power transfer methods and their associated restraint gradients. Analysis of isolation options show that the NASA requirements may be met using active and passive isolators to varying degrees. An ideal active isolator can

TABLE 1. SSP MICROGRAVITY MISSION REQUIREMENTS OPTIONS

DESIGN OPTIMIZATION: MICROGRAVITY MISSION ACCOMMODATION			
OPTIONS: CORE SS VECTORIAL RESULTANT* MAXIMUM ACCELERATION LEVELS AT APPLICABLE EXPERIMENTS, MISSION PAYLOADS AND MTL			PERIOD OF DURATION AND NUMBER OF PERIODS
1.	$10^{-5} G_0$ AS CURRENTLY STATED IN PDRD		30 DAYS MINIMUM
2.	$10^{-6} G_0$ 0 $H_z < F < 0.032 H_z$ $10^{-5} G_0 F$ <hr style="width: 50%; margin-left: 0;"/> 0.32 Hz      0.032 $H_z < F < 3.2 H_z$ $10^{-4} G_0 F^2$ <hr style="width: 50%; margin-left: 0;"/> (3.2 Hz) <sup>2</sup> 3.2 $H_z < F$		TARGET OF 9 PERIODS PER YR
3.	$10^{-7} G_0$ 0 $H_z < F < 0.032 H_z$ $10^{-6} G_0 F$ <hr style="width: 50%; margin-left: 0;"/> 0.32 Hz      0.032 $H_z < F < 3.2 H_z$ $10^{-5} G_0 F^2$ <hr style="width: 50%; margin-left: 0;"/> (3.2 Hz) <sup>2</sup> 3.2 $H_z < F$		90 MINUTES MINIMUM  TARGET OF 18 PERIODS PER YR
<p>* THE VECTORIAL RESULTANT INCLUDES DRAG, GRAVITY GRADIENTS, ORBITAL LVLH FLIGHT, STATION MANEUVERS, PERIODIC/NON-PERIODIC DISTURBANCES, AND RESONANCES.</p> <p>F = FREQUENCY</p>			

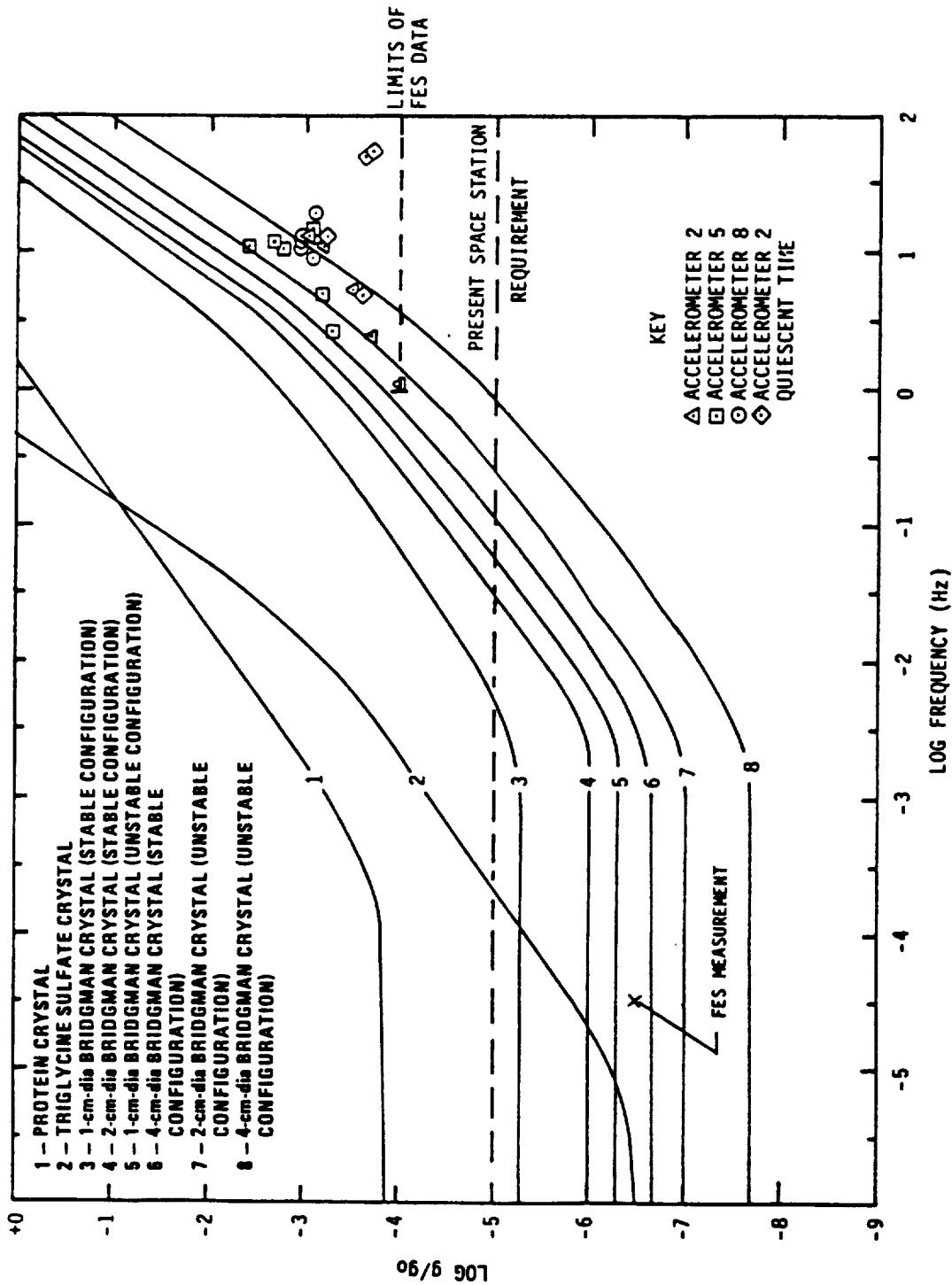


FIGURE 1. EXAMPLE MICROGRAVITY REQUIREMENTS RELATED TO PROCESS

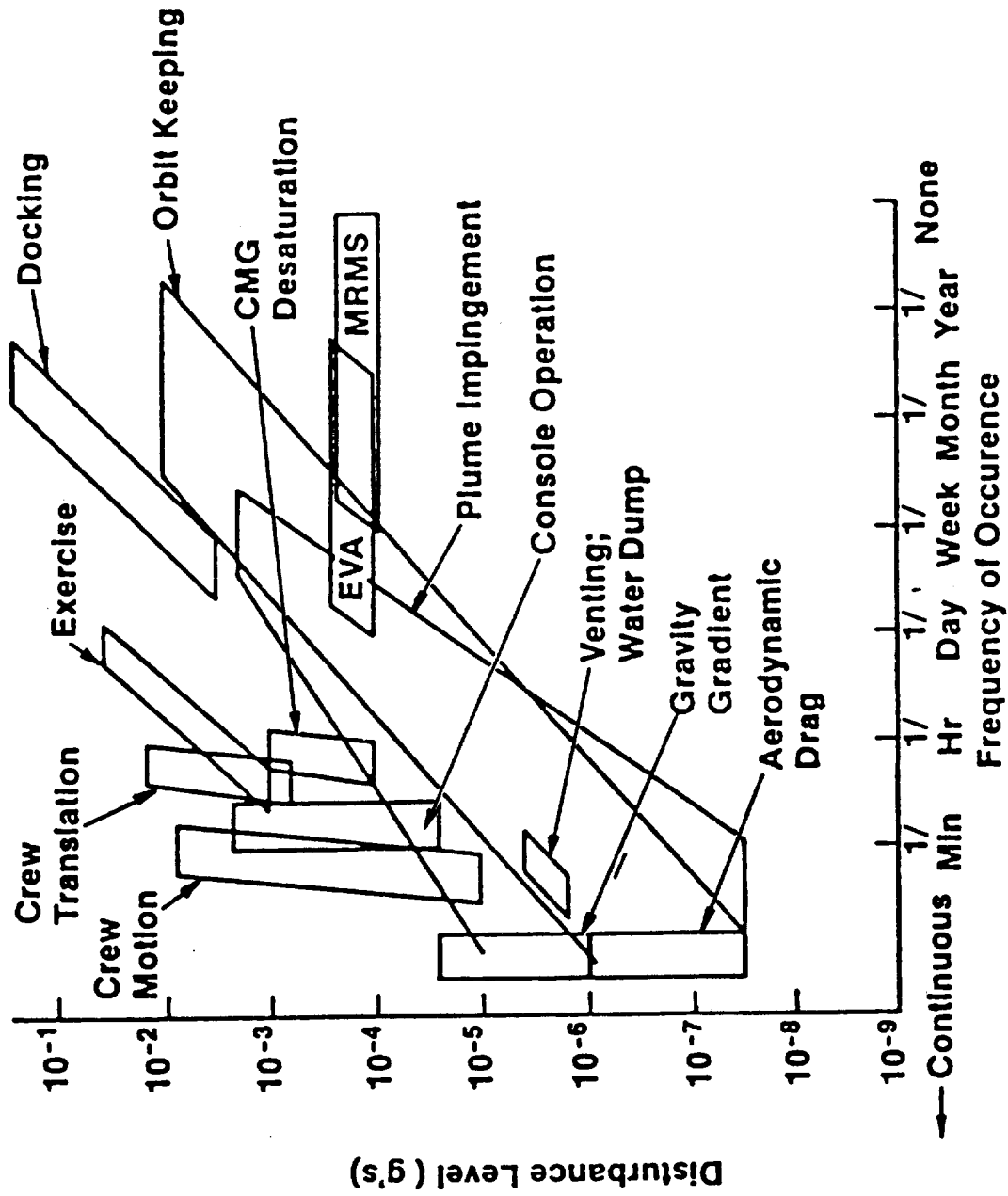


FIGURE 2. TYPICAL DISTURBANCE ENVELOPES

satisfy the isolation requirements for all three options for low and high crew disturbance levels depending on the value of  $\xi$ . Analysis results are shown in Table 2.

Three isolation candidates are identified: passive mechanical, active servo; lead network and active servo; accelerometer. The passive mechanical system is possibly the lightest and cheapest system, but is sensitive to high-frequency input, is less versatile and sensitive to restraint (i.e., flex lines) gradient forces. The active network, lead network option is not as sensitive to high frequency outputs and is more versatile, but remains heavy, expensive, and sensitive to restraint gradient forces. The active servo accelerometer option is less sensitive to high-frequency inputs and restraint gradient forces and is versatile. But it too is heavy and expensive. Available accelerometers are the topic of another workshop paper. Two technical approaches offering the promise of reduced package size and weight are presented in the remainder of this paper. They are the design concept for an optical cavity-locking accelerometer and the technology for an integrated silicon accelerometer. Each approach is discussed in a section which follows.

### III. THE CAVITY-LOCKING ACCELEROMETER (CLA)

Most accelerometer concepts considered to date use electrical pick-off schemes to detect the pendulum deflection under acceleration. Thus the accelerometer sensitivity is limited by the electronic pick off sensitivity. This limitation also dictates a 'sizable deflection of the pendulum structure for the accelerometer to respond to a given acceleration. The required deflection causes stress in the pendulum which enhances and propagates micro-creeps leading to bias problems under changing temperatures or as a result of aging.

One solution to this problem is to employ a pick-off technique with much higher sensitivities thereby reducing the pendulum deflection requirements for a given acceleration. Such a pick-off technique allows the use of a much thicker flexure or diaphragm structure which reduces the amount of stress developed in the structure. The Cavity-Locking

TABLE 2. MICRO-G ISOLATION ANALYSIS ISS RESULTS

CREW MOTION (STOCHASTIC)	IDEAL ISOLATOR CHARACTERISTICS	$\mu$ GRMS @ EXP	SATISFIES SPEC. OPTION
<p>QUIESCENT MOTION LOW-LEVEL (CASE B)</p> <ul style="list-style-type: none"> <li>• Console Ops</li> <li>• Resp, Cough, Sneeze</li> <li>• Arm Motion</li> <li>• Leg Motion</li> <li>• Swaying Motion</li> </ul> <p>RMS = 24.8<math>\mu</math>G @ HAB</p>	<p>PASSIVE ISOLATOR <math>\omega = .0062, \xi = .5</math></p> <p>PASSIVE ISOLATOR <math>\omega = .0062, \xi = .2</math></p> <p>ACTIVE ISOLATOR <math>\omega = .0062, \xi = .7</math></p>	<p>1.30</p> <p>0.26</p> <p>0.02</p>	<p>1, 2</p> <p>1, 2</p> <p>1, 2, 3</p>
<p>UNINHIBITED MOTION HIGH-LEVEL (CASE A)</p> <ul style="list-style-type: none"> <li>• Torso Bowing</li> <li>• Crouch &amp; Push-Off</li> <li>• Arm Flapping</li> </ul> <p>RMS = 105.0<math>\mu</math>G @ HAB</p>	<p>PASSIVE ISOLATOR <math>\omega = .0062, \xi = .5</math></p> <p>PASSIVE ISOLATOR <math>\omega = .0062, \xi = .2</math></p> <p>ACTIVE ISOLATOR <math>\omega = .0062, \xi = .7</math></p>	<p>2.90</p> <p>0.58</p> <p>0.03</p>	<p>1</p> <p>1, 2</p> <p>1, 2, 3</p>

Accelerometer (CLA) holds such a promise by virtue of its optical pick off technique which provides for several orders of magnitude increase in sensitivity. It will be shown here that the CLA can lead to accelerometers with nano-g ( $10^{-9}$  g) sensitivities while using rather thick diaphragms which should improve the bias stability.

The operational principle of CLA is based on tracking the resonance frequency of an optical (Fabry-Perot type) cavity. As shown in Figures 3 and 4, a probe beam provided by a coherent source (such as a laser diode) is injected into the cavity and the transmitted output of the cavity is measured by a photodetector. The strategy in the CLA is to assure that the frequency of the probe beam matches a resonance frequency of the interferometer cavity at all times. This can be accomplished either by adjusting the cavity length (as in Figure 3) so that the cavity resonance frequency matches the probe beam frequency or by adjusting the probe frequency (as in Figure 4), to match the cavity resonance frequency.

The cavity consists of two parallel mirrors with one mirror being attached to, or part of, a flexible diaphragm. A beam of light injected into the cavity undergoes multiple reflections and an output port is formed which is a function of the separation between the two mirrors as well as their reflectivities. Figure 5 shows such an output as a function of mirror separation for a number of different mirror reflectivities. It is seen that the intensity output exhibits successive peaks as the mirror separation changes by one-half of the probe beam wavelength. Furthermore, the peaks become sharper and sharper as reflectivity of the mirrors is increased. The peaks correspond to the resonance condition of the input (probe) beam frequency and the cavity length.

Acceleration along the cavity axis induces an inertial force in the diaphragm mirror, causing diaphragm deflection. This is followed by a change in cavity length which disturbs the resonance condition. An error signal is generated by the photodetector and the control loop restores the resonance condition. As stated earlier, the error signal can be applied to a PZT attached to the diaphragm thus driving the

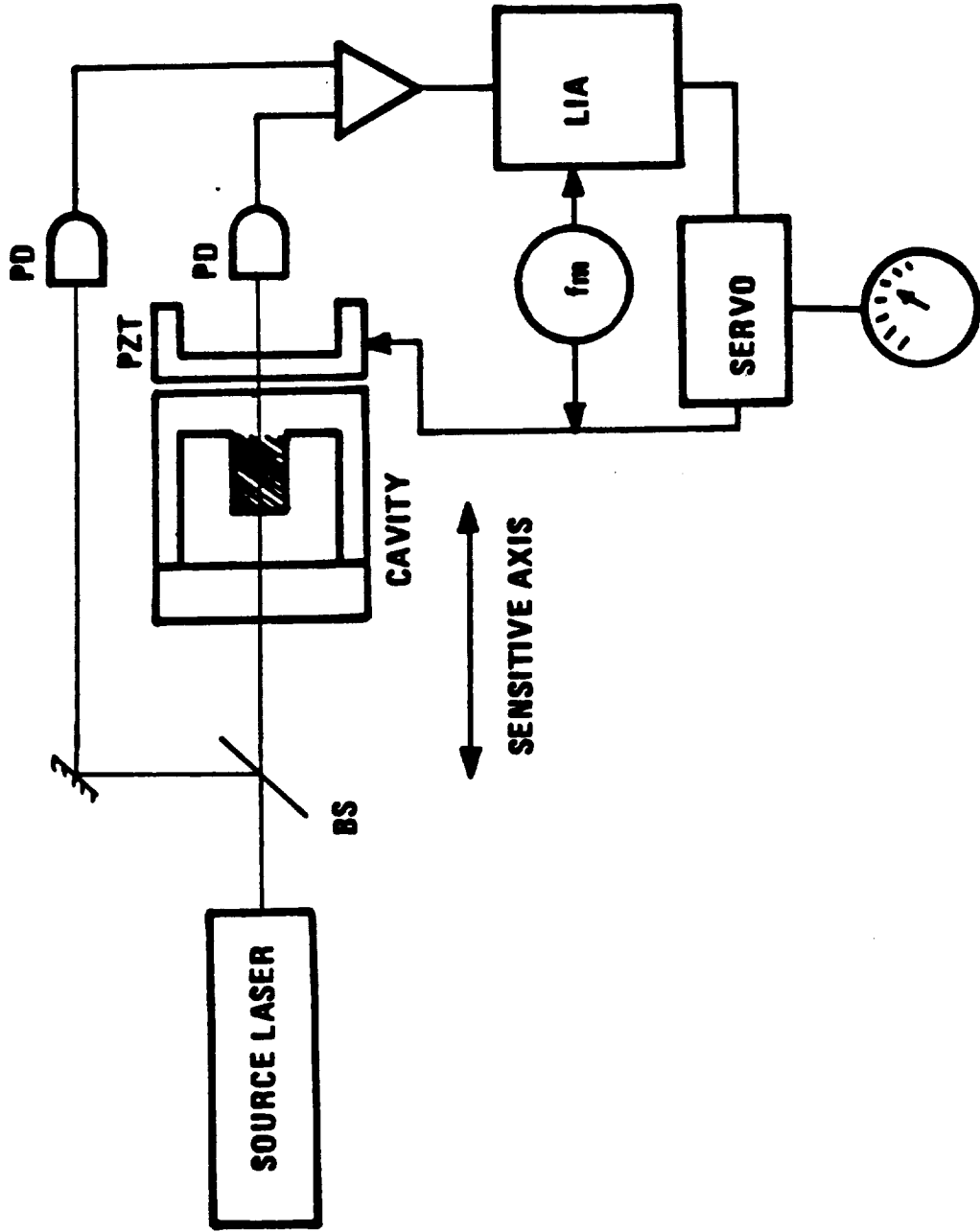


FIGURE 3. SCHEMATICS OF THE CLA WITH THE CAVITY LENGTH CONTROL TECHNIQUE

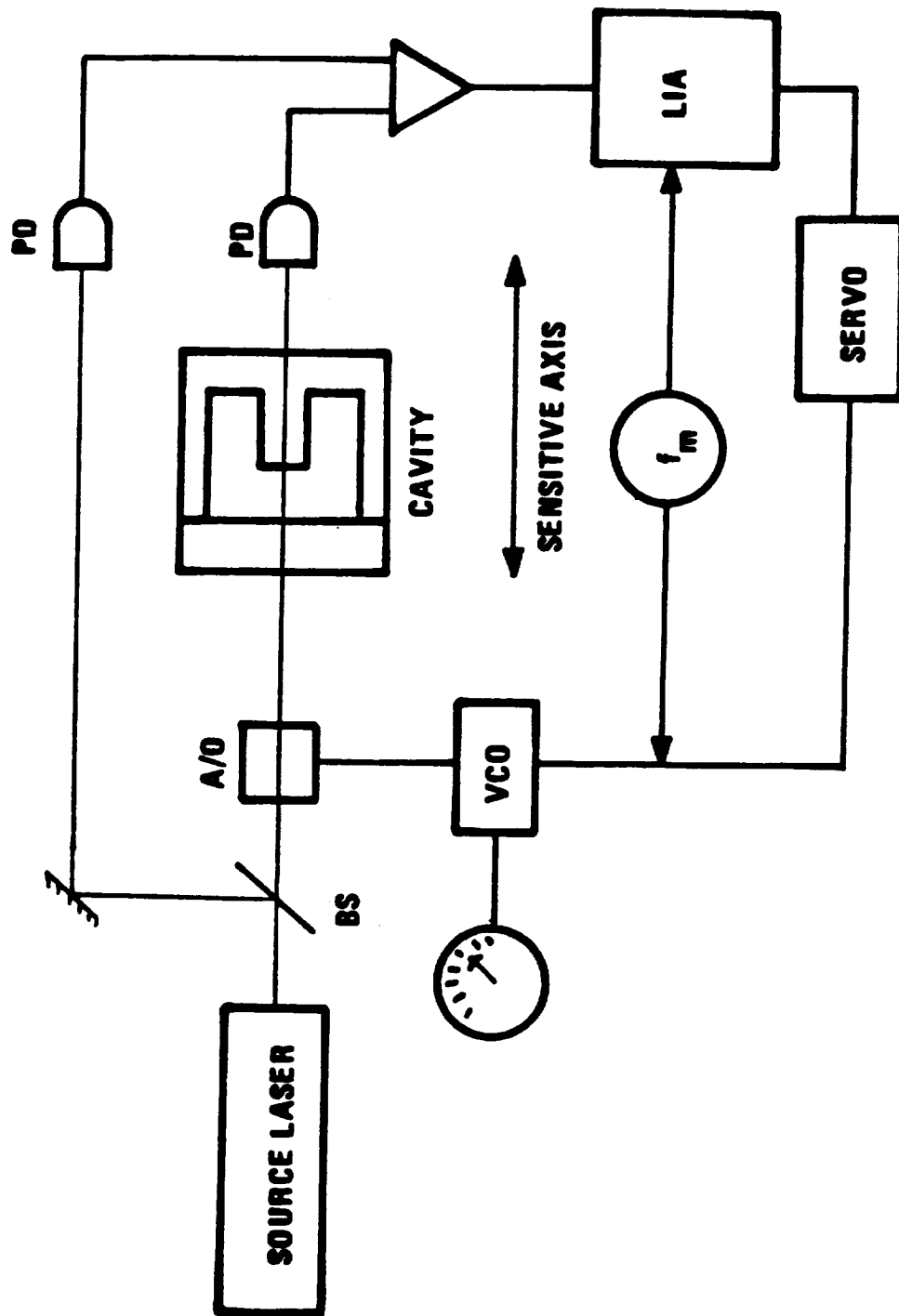


FIGURE 4. SCHEMATICS OF THE CIA WITH THE PROBE BEAM CONTROL FREQUENCY

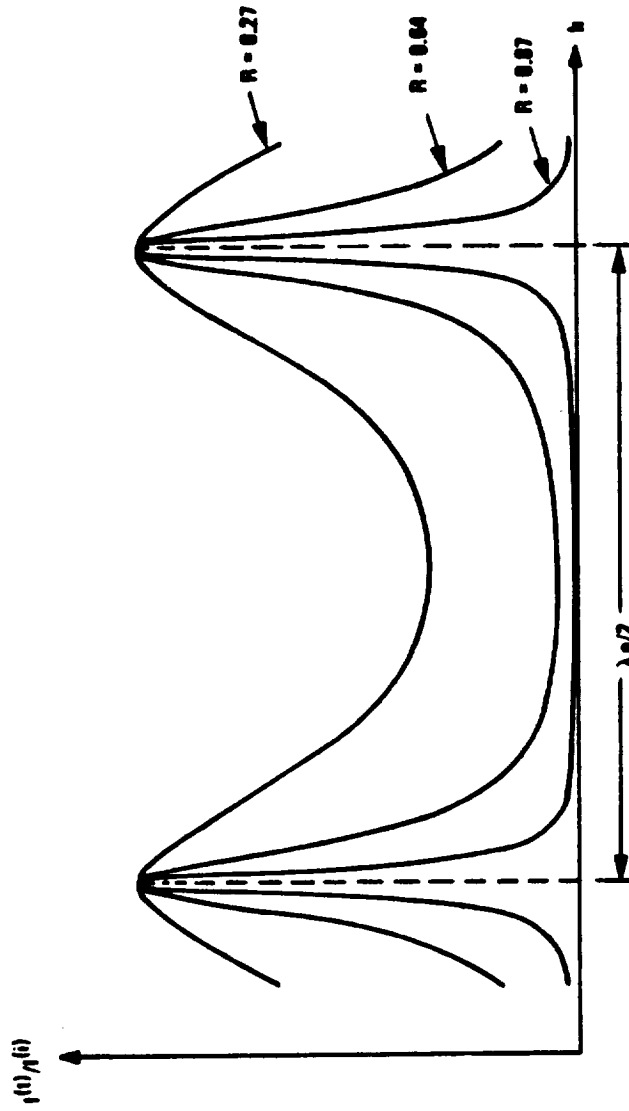


FIGURE 5. OUTPUT OF THE INTERFEROMETER AS A FUNCTION OF MIRROR SPACING

cavity length to the resonance condition or to an acousto-optic frequency shifter adjusting the probe beam frequency. A phase sensitive detection technique is used to achieve the resonance tracking. This technique which has been successfully employed in passive cavity gyros<sup>(1)-(3)</sup>, is the main ingredient in achieving the high sensitivities in the CLA. Thus, referring to Figure 3, a modulating signal at a frequency  $f_m$  is applied to the PZT that scans the cavity length around its resonance and with an amplitude corresponding to the cavity linewidth (the resonance width in Figure 5). The detector output is demodulated at the same frequency by the phase sensitive detector (shown as LIA in Figure 3). Any departure of the cavity length from its resonance condition generates an error signal at  $2f_m$  which is converted to a dc signal after demodulation. The dc signal is then applied to the PZT that restores the resonance. In Figure 4, the modulation and the error signals are applied to a frequency shifter that restores the resonance condition by adjusting the probe beam frequency. In either case, a second detector is used to monitor the probe beam intensity, and its output is subtracted from that of the first before demodulation. This provides for the common-mode rejection of changes in probe beam intensity.

Sensitivity Analysis. Sensitivity of the CLA is determined by the diaphragm configuration and the photodetection sensitivity. It has been demonstrated in passive cavity gyros that the detector shot noise is the main mechanism for limiting the photodetection sensitivity. We use the detector shot noise as the limiting mechanism of the CLA sensitivity.

Using the deflection equation of a circular diaphragm<sup>(4)</sup> and the detector shot noise equation, it can be shown that the acceleration sensitivity of the CLA is given by

$$S = \frac{8Et^3 (1 - R)}{3\pi (1 - \nu^2)a^2 M} \frac{\lambda}{\sqrt{N\eta\tau}}$$

where

- S = acceleration sensitivity
- t = diaphragm thickness
- a = diaphragm radius
- E = Young's modulus of diaphragm
- $\nu$  = Poisson's ratio of diaphragm
- M = mass of diaphragm mirror
- $\lambda$  = wavelength of light source
- N = number of photons per second incident on the detector
- $\eta$  = detector quantum efficiency
- $\tau$  = detector integration time
- R = reflection coefficient of interferometer mirrors.

As an example, if a CerVit diaphragm is used for which  $E = 13.37 \times 10^6$  psi and  $\nu = 0.252$ , and if  $t = 0.1$  in.,  $M = 10$  gr.,  $\lambda = 0.8 \mu\text{m}$ ,  $R = 0.995$ ,  $\eta = 0.8$ ,  $\tau = 1$  sec, and also  $N = 4 \times 10^{15} \text{ sec}^{-1}$  (corresponding to an incident power on detector of 1 mw), we obtain from Equation (1):

$$S = 1.54 \times 10^{-9} \text{ g} \quad (2)$$

Notice that such a sensitivity is achieved with a diaphragm whose thickness is 0.1 in., which is much thicker than the ones used in conventional accelerometers. Since the magnitude of stress in a loaded diaphragm is proportional to the inverse square of the diaphragm thickness<sup>(4)</sup>, we expect the stress levels in the CLA be much reduced compared to conventional accelerometers which should alleviate the bias problems associated with the stress.

Dynamic Range. The maximum acceleration that the CLA can measure depends on the particular scheme of its resonance frequency tracking. In the configuration of Figure 3, where the control loop signal is applied to the PZT to rebalance the diaphragm and maintain the cavity length on resonance, the maximum applied acceleration depends on the operational range of the control loop. This is essentially an

electronic design issue which can be determined in a trade-off study of the control loop parameters. On the other hand in the configuration of Figure 4, where the error signal is used to adjust the probe beam frequency and the diaphragm is allowed to deflect, it is the tuning bandwidth that determines the maximum acceleration. It can be shown that the maximum allowable acceleration,  $\gamma_{max}$ , for a given bandwidth is given by

$$\gamma_{max} = \frac{16\pi E t^3 h}{3(1 - v^2) a^2 M} \left( \frac{\delta\lambda}{\lambda} \right) \quad (3)$$

where

$h$  = nominal distance between the cavity mirrors,

$\delta\lambda$  = tuning bandwidth of the probe beam.

All other parameters are the same as defined in Equation (1). The important parameter, from a component availability standpoint, is  $\delta\lambda$ . Tunable laser diodes are now available with a tuning bandwidth of 100 Angstroms. The frequency tuning in these diodes is achieved by varying the excitation current to the laser diode. The probe beam frequency can also be adjusted via the acousto-optic device, as shown in Figure 4. The frequency bandwidth of the available acousto-optic devices is limited to few gigahertz which corresponds to a  $\delta\lambda$  of few hundredth of an Angstrom.

As an example, a frequency shifter with 3 GHz bandwidth yields a  $\delta\lambda = 0.064$  Angstroms. Using the same parameter values as in the sensitivity analysis and with  $h = 1$  cm we obtain from Equation (3)

$$\gamma_{max} = 34 \text{ g} \quad (4)$$

Much higher accelerations can be measured if tunable laser diodes are used.

Although a good deal of experimentation and further analyses are needed to fully assess the potentials of the CLA, the concept does promise a significant improvement in sensitivity and bias stability based on the analysis presented here. These improvements are direct results of the optical pick-off technique employed in the CLA. As was

shown here, acceleration measurement sensitivities of the order of nano-g are possible using very thick diaphragms which develop much less stress during the accelerometer operation. Furthermore, such thick diaphragms are much less prone to micro-creeps and other damages during fabrication. If, as is often stated, such micro-creeps are the primary cause of the bias shifts then the thick diaphragms used in the CLA should provide it with much improved bias stability.

Finally, the CLA offers an interesting possibility for an all optical inertial navigation systems. If ring laser gyros (RLGs) are used in such systems, the probe beam of the CLA is already provided by one of the single beam output of an RLG. This would eliminate the need (and the corresponding cost) for highly stable coherent light source needed for the operation of the CLA.

#### IV. THE INTEGRATED SILICON ACCELEROMETER (ISA)

The ISA is an inertial grade accelerometer under development at Honeywell for application in strapdown RLG navigation systems. It is to be operated without temperature control, and contains no liquids, so as to be operational immediately after being turned on.

General Description of the Accelerometer. This is a pendulous accelerometer with torque rebalance. As shown in Figure 6, the pendulum is formed of single-crystal silicon, into which flexures are etched to provide suspension with a low stiffness. Mounted on the pendulum are rebalance coils, these coils and their bobbins forming most of the seismic mass. Pick-off of the pendulum deflection, to generate an error signal for rebalance, is by piezo resistive strain elements implanted into the flexures. Electronics for rebalance is processed directly on the silicon pendulum using existing IC technology (see Figure 7). The pendulum is sandwiched between two end caps which are bonded to it to form a capsule. The separation between the pendulum assembly and the end caps is small so that narrow gaps are formed, providing gas damping of the pendulum. This permits safe handling of the accelerometer when it is not operating.

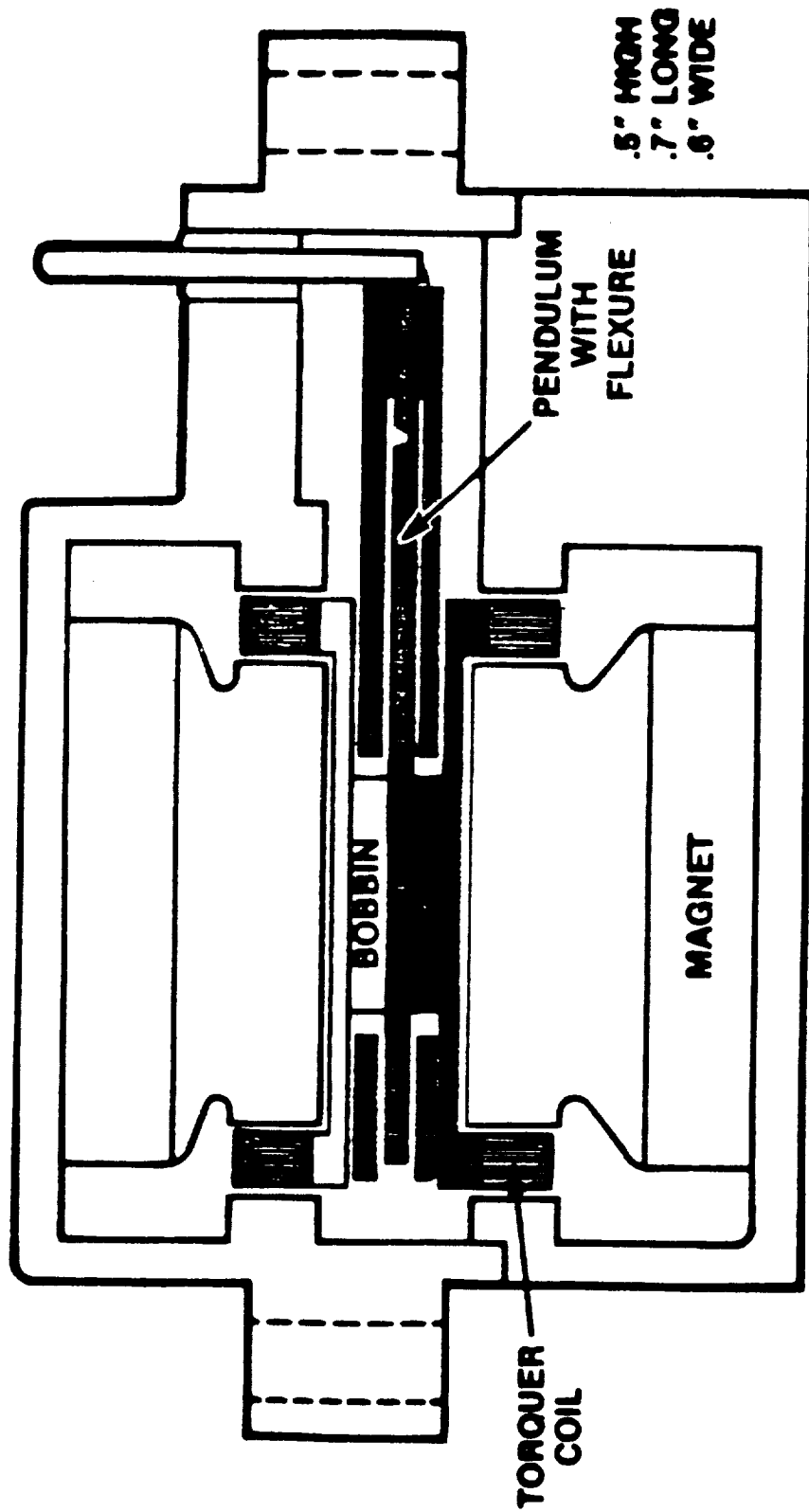


FIGURE 6. CROSS SECTION OF THE ISA

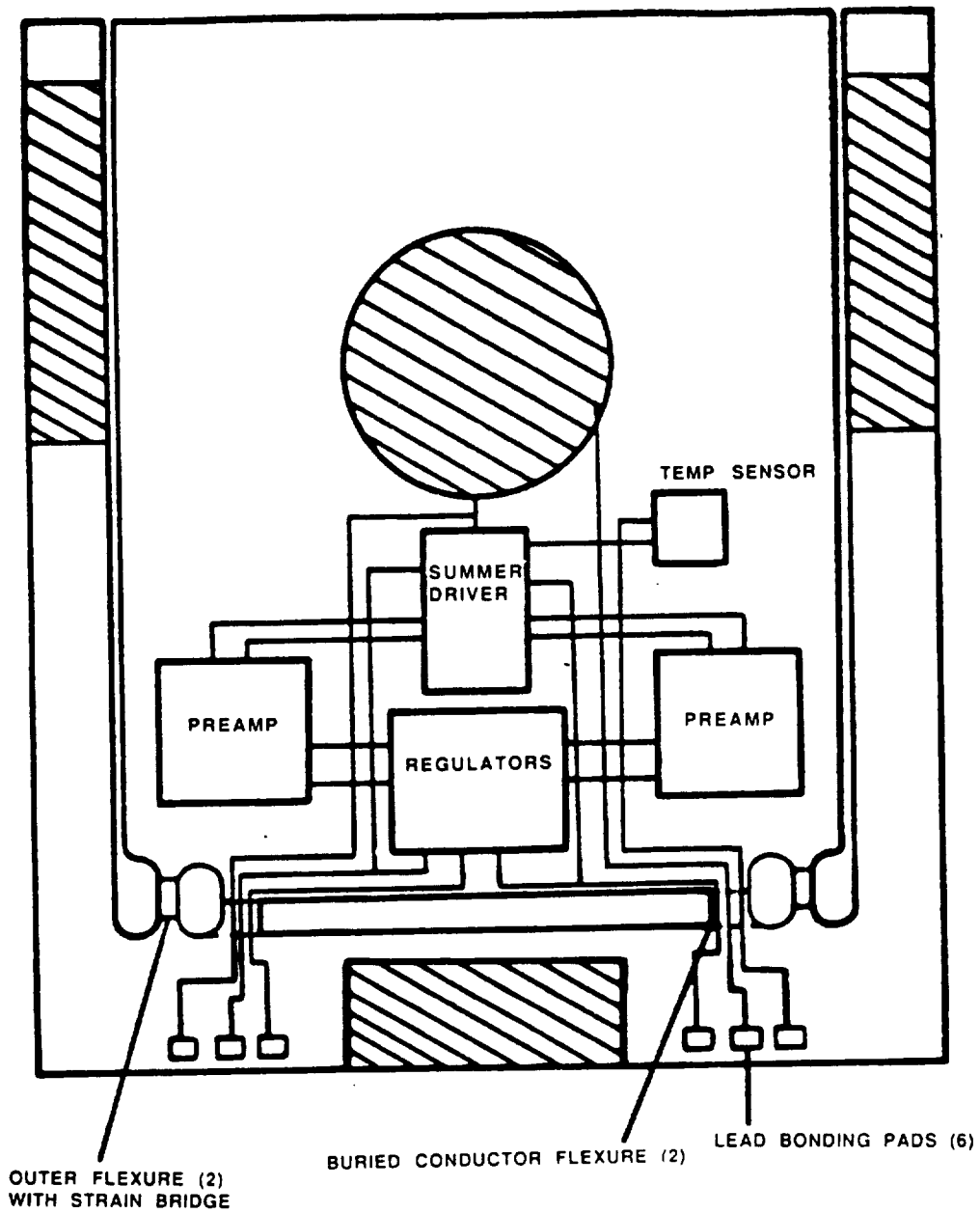


Figure 7. Schematics of the ISA Pendulum with On-board Electronics

The capsule is assembled into two Samarium Cobalt magnet assemblies which act also as the accelerometer case. Figure 8 shows the cut-away schematics of the assembly. Rebalance currents in the torque coils, in the fields of the magnets, produce the rebalance torque. The current through the torquer is an analog measure of the input acceleration. With analog-to-frequency conversion, the output is in a form suitable for the digital operations of a navigation system computer.

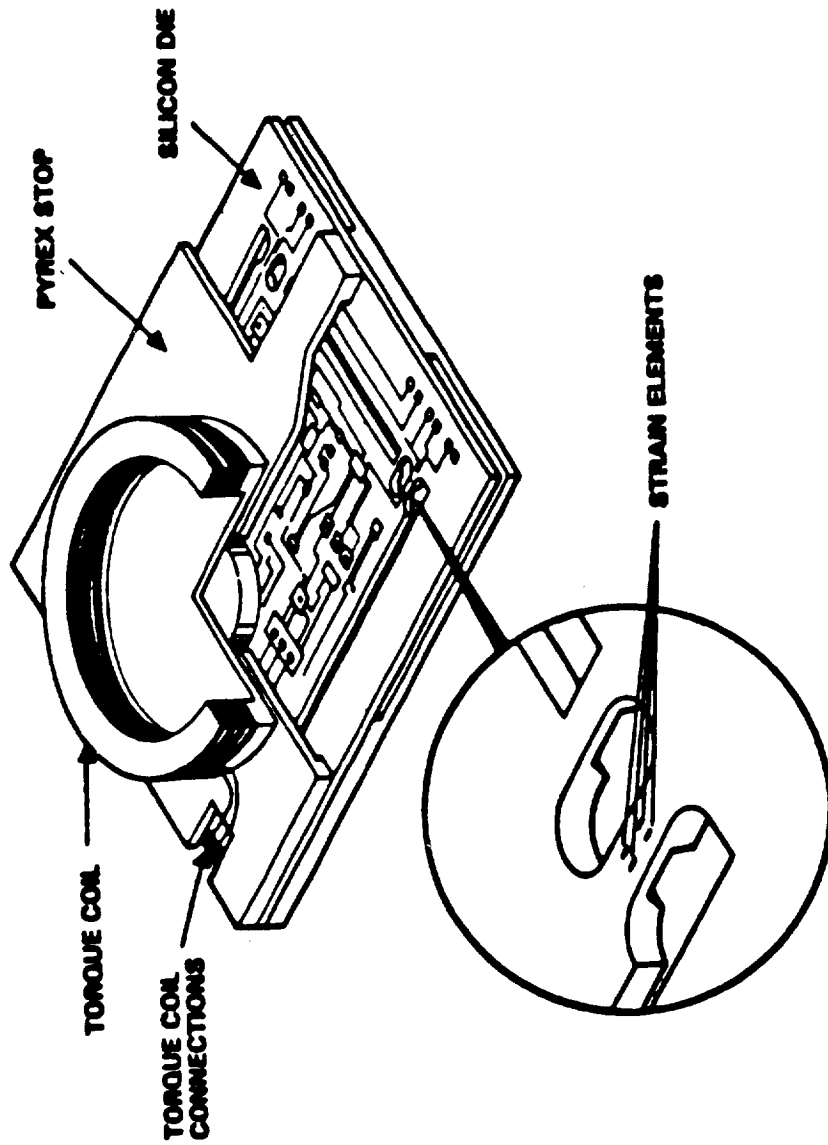
Development Goals. Goals for the development are roughly one order of magnitude beyond the state of the art in strapdown, fast reaction accelerometers without temperature control. Bias stability goals are 10 micro g's, (one sigma) short term and 20 micro g's, long term. The short term scale factor stability goal is 10 parts per million. Temperature sensitivity goal is 0.5 ppm per degree C, with software compensation. Input axis alignment stability goals are 5 micro radians short term, and 20 micro radians, long term.

The larger of two feasibility models now being evaluated measures 0.6 x 0.7 x 0.5 in.; this may be reduced in future development. It weighs 38.5 grams. The smaller unit weighs 20 grams.

The current breadboard results with the electronics off of the pendulum show an acceleration sensitivity of 1 micro-g. The limitation on sensitivity is mostly due to electronics noise. Detailed short- and long-term bias stability measurements are in progress.

## V. CONCLUSION

Space Station micro-g performance goals are achievable through the management of operation, the design of isolation systems, and the use of accelerometers in active servo loops. New accelerometer designs are available to meet system micro-g requirements with reduced impact on system size, weight, and power.



Silicon Sensing Capsule

FIGURE 8. CUT-AWAY SCHEMATICS OF THE ISA ASSEMBLY

#### REFERENCES

1. S. Ezekiel and S. R. Balsamo, Appl. Phys. Lett. 30, 478 (1978)
2. G. A. Sanders, M. G. Prentiss, and S. Ezekiel, Opt. Lett. 11, 569 (1981)
3. M. M. Tehrani and J. A. Hoschette, Proc. SPIE, Vol. 412, P. 234 (1983)
4. R. J. Roark and W. C. Young, Formulas for Stress and Strain, Fifth Edition, McGraw-Hill Inc. (1975)